J Mater Sci (2010) 45:2112–2117
DOI 10.1007/s10853-009-4131-2

HTC2009

Improvement of the wettability of SiMn IF-HSS by liquid zinc by controlling the dew point of the annealing gas atmosphere

Joonho Lee · Joongchul Park · Yunkyum Kim · Sun-Ho Jeon

Received: 29 May 2009 / Accepted: 16 December 2009 / Published online: 30 December 2009

Abstract The wettability of low-carbon, 0.3 wt%Si–0.4 wt%Mn interstitial-free steel by liquid zinc at 450 °C was investigated using the dispensed sessile drop method. Before the wetting tests, the steel samples were annealed in a 15%H_2–Ar gas atmosphere at three different dew points, namely −60, −40, and 0 °C. It was found that as the dew point was increased from −60 to −40 °C, the wettability became poorer. However, as the dew point was increased further to 0 °C, the wettability was dramatically improved and was better than that of −60 °C. In order to understand the dramatic change in wettability, the surfaces of the steel samples after annealing were analyzed with SEM and TEM. It was found that the surface oxide changed from randomly distributed hemisphere particles of 20–30-nm high on a very thin oxide film to a film-like layer ~15-nm thick as the dew point was increased from −60 to −40 °C, and at the dew point of 0 °C, internal oxidation was so pronounced that a very thin surface oxide layer 1–2-nm thick was formed. It was believed that the improvement of the wettability at the dew point of 0 °C was caused by the short diffusion distance in the surface oxide layer.

Introduction

In order to increase the strength of interstitial-free (IF) high strength steel (HSS), generally Mn and Si are added as alloying elements, because the addition of Mn and Si improves the most significant mechanical properties at a low cost [1–3]. However, during the annealing of IF-HSS containing Mn and Si, Mn and Si can segregate on the steel surface to form nanometer-sized oxides such as MnO, $MnSiO_3$, Mn_2SiO_4, and SiO_2 [4–7]. These oxides show poor wettability by liquid zinc ($\theta > 90°$), whereas the steel matrix shows good wettability ($\theta < 90°$) [3]. Therefore, it is expected that as the fraction of surface oxides increases, the wettability will become poorer [8]. Accordingly, knowing how to control the morphology of the surface oxides is very important to improve the wettability of the IF-HSS plates containing Mn and Si.

The wetting characteristics of steel by liquid zinc and zinc alloys have mainly been investigated using the meniscograph method [9]. The meniscograph method measures the wetting behavior after the steel plate has been immersed in a liquid zinc bath for a certain period of time. When IF-HSS is applied, the equilibrium wetting force (or contact angle) can be achieved in more than 20–30 s [10]. Since a conventional hot-dip galvanizing process is finished in 5–10 s, this method is not suitable for the evaluation of wettability of IF-HSS by zinc and zinc alloys. As an alternative method, the dispensed sessile drop method using a high-speed video camera was employed by several researchers [11–14]. We recently investigated the wettability of IF-HSS by changing the Si concentration at a fixed Mn content, and found that 0.3 wt%Si–0.4 wt%Mn IF steel showed the best wetting behavior among the tested samples [4]. The improvement in the wetting characteristic was possible by the modification of the morphology of the surface oxides. However, even with this sample, the contact angle at 5 s was as high as 80°, which is not suitable for the hot-dip galvanizing process. Therefore, a further modification of the surface oxide morphology is required.

J. Lee (✉) · J. Park · Y. Kim
Department of Materials Science and Engineering, Korea University, 5 Anam-dong, Seongbuk-gu, Seoul 136-713, Korea
e-mail: joonholee@korea.ac.kr

S.-H. Jeon
POSCO Technical Research Laboratories, Gwang-yang, Chunranam-do 545-090, Korea

In this study, we tried to modify the surface oxide morphology of the 0.3 wt%Si–0.4 wt%Mn IF-HSS plate by changing the dew point in the annealing gas atmosphere. The wetting tests were carried out using the dispensed sessile drop method, and the surface oxide morphology was analyzed with a scanning electron microscope (SEM) and a transmission electron microscopy (TEM) with an energy dispersive spectrometer (EDS).

Experimental

The steel plate used in the present experiments was prepared in a vacuum-induction furnace. Hot-rolled plate went through pickling, cold-rolling (to 0.8-mm thick with a reduction rate of 73%), and degreasing. This sample was used in the experiments without polishing. Table 1 shows the chemical analysis result of the steel sample used in this study. After a conventional rolling process, a steel plate (120 mm × 250 mm × 1.4 mm) was obtained. After the steel plate was placed in a simulator (HDG simulator, Iwatani, Germany), the furnace was heated to 800 °C under a 15%H_2–N_2 atmosphere with a controlled water partial pressure (see Table 2) at a heating rate of +5 °C/s. It was then maintained at 800 °C for 40 s, and then cooled to 500 °C at a cooling rate of −15 °C/s. It was held at 500 °C for 300 s, and then cooled by a rapid flow of nitrogen gas (2 l/s), yielding a cooling rate of −20 °C/s. After an annealing process, the sample was sectioned into 20 mm × 20 mm plates. These plates were used in the wetting experiments, SEM (JEOL, JSM-6700F) analysis, and TEM (JEOL, JEM-2100, 200 keV) analysis. The TEM samples were prepared using FIB (FEI, Nova200, 30 keV, ~100-nm thick).

For the dynamic reactive wetting experiments, a lab-made dispensed sessile drop test machine was employed. Details were described in Ref. [4]. Here, we describe the general experimental procedure. In a cross-shaped quartz reaction tube, a sessile dropper assembly is placed 4 mm above the steel plate. The furnace was made up of kanthal heating elements, and the maximum temperature of the furnace was 1000 °C. The furnace temperature was monitored by two K-type thermocouples, which were located in the upper zinc bath (99.99% purity) and just below the steel plate. The temperature difference between these two thermocouples was less than ± 2 °C. The wetting experiments were carried out at 450 °C. The furnace was heated to 450 °C at a heating rate of +5 °C/s, and was held at this temperature for 30 min. Then a droplet of liquid zinc (~0.2 g) was dispensed onto the steel plate. Once a liquid droplet was dropped onto the steel plate (the impacting velocity ranges between 0.11 and 0.31 m/s), the wetting behavior was investigated with two different CCD cameras: a high-speed digital camera at a recording rate of 3000 fps and a typical high-resolution CCD camera at a recording rate of 6 fps. The light beam from a single light source (LED lamp) was split into two different cameras to investigate the wetting behavior on the different timescales. During the experiments, a purified hydrogen gas atmosphere was maintained.

Table 1 Chemical composition of the steel plate used in the present study

Element	C	Si	Mn	P	Al
wt%	0.005	0.3	0.4	0.08	0.05

Table 2 Water vapor pressure at each due point

DP (°C)	0	−40	−60
P_{H_2O} (atm)	5.976×10^{-3}	1.782×10^{-4}	1.700×10^{-5}

Results and discussion

Contact angle versus time

In Fig. 1a, the contact angles from 0 to 600 s are shown with respect to time on a logarithmic scale. (Here, only selected data points were plotted, but these data points are sufficient to explain the dynamic reactive wetting behaviors. The experimental error of the contact angle measurements was ±5°.) For a better understanding of the initial wetting behavior, the contact angles from 0 to 100 ms are separately shown in Fig. 1b. It was found that by 100 ms the oscillation of contact angle was considerable, and diminished when $t > 1$ s. During the initial 100-ms period, the contact angle for the three different samples varied between the advancing angle (upper limit) and the receding angle (lower limit). In this study, the mean value of advancing and receding contact angles is assumed to be a quasi-equilibrium angle characterizing wetting at very short time ($t \approx 0$ s). The quasi-equilibrium angles at $t \approx 0$ s for the three samples at dew points (DPs) of −60, −40, and 0 °C were estimated to be 105°, 120°, and 100°, respectively. Thereafter, the contact angle gradually decreased over time. The dynamic contact angles at $t = 5$ s for the three samples at DPs of −60, −40, and 0 °C were estimated to be 87°, 116°, and 55°, respectively. The dynamic contact angles at $t = 50$ s for the three samples at DPs of −60, −40, and 0 °C decreased to 84°, 103°, and 17°, respectively. Accordingly, regardless of the wetting time, the contact angle of the steel plate annealed at a DP of 0 °C showed the best wetting behavior, and that of the steel plate annealed at a DP of −40 °C showed the worst.

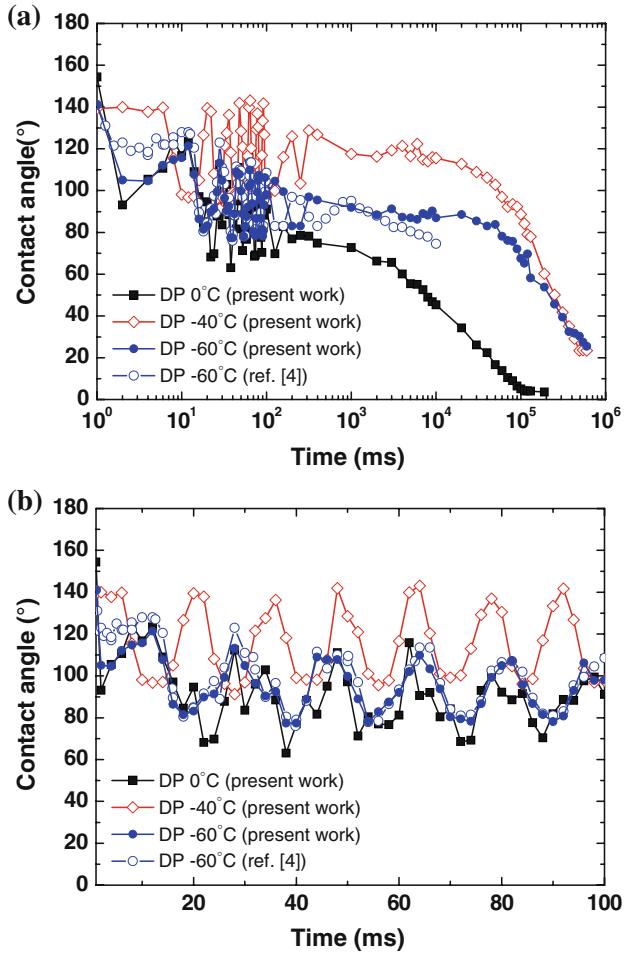

Fig. 1 Change in contact angle between steel plate and liquid zinc over time: **a** whole wetting period (0–600 s), **b** initial period of wetting (0–100 ms)

At $t = 0$ s, it is believed that the effect of the chemical reaction between liquid zinc and steel substrate on the contact angle was negligible, so that the initial contact angle can be determined from the surface chemistry. Consequently, it is believed that due to the poor wettability in the initial stage ($\theta > 90°$) all the three samples were covered by surface oxide layers. Generally, as the dew point increases, the driving force to form oxides increases. Accordingly, one may expect that the contact angle would increase as the dew point is increased. However, when the selective oxidation occurs, the wetting behavior can be improved by increasing the dew point. Several researchers already mentioned this issue [5, 15–17]. In the present study, the wettability of the steel plate annealed at the dew point of 0 °C showed the best performance among the tested samples. In order to understand this wetting behavior, the surface oxide was analyzed using SEM and TEM. The results are given in the following section.

SEM and TEM analyses

In Fig. 2, the SEM images of the surface of the annealed samples are shown. For the sample annealed at a DP of −60 °C (the sample reported in our previous report [4]), the surface oxide appeared as small spheres approximately 80 nm (25–300 nm) in diameter. As the annealing dew point increased to −40 °C, the oxides formed irregular smaller particles. At the annealing dew point of 0 °C, it became very difficult to distinguish the surface oxides from the bare metal surface. Therefore, it was difficult to describe the contact angle as a function of the oxide coverage on the steel surface.

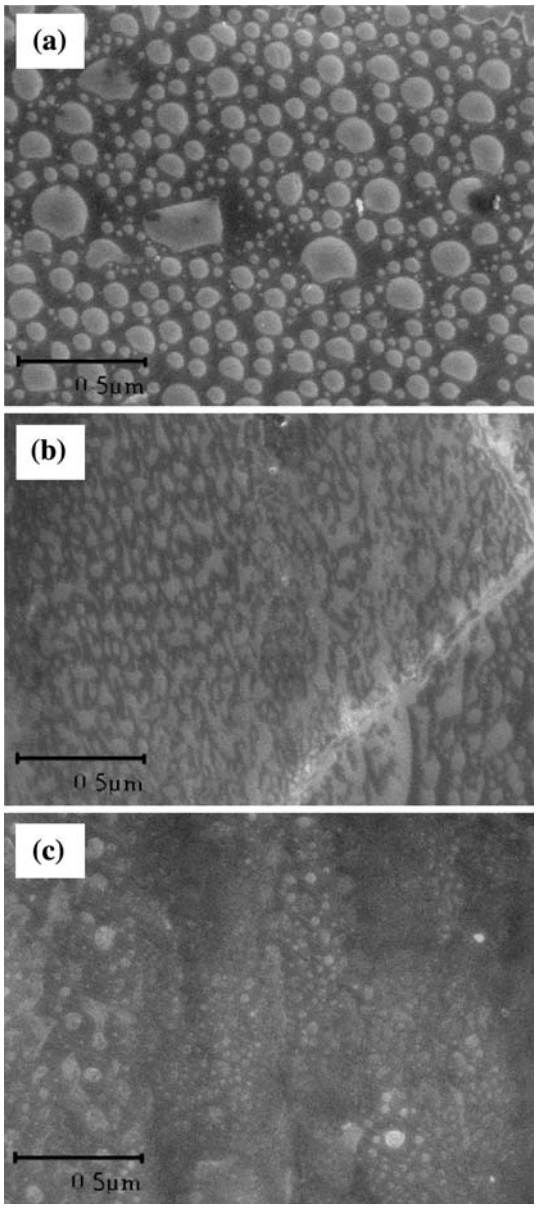

Fig. 2 Surface morphology of the steel plate annealed at **a** DP −60 °C, **b** DP −40 °C, and **c** DP 0 °C investigated with SEM

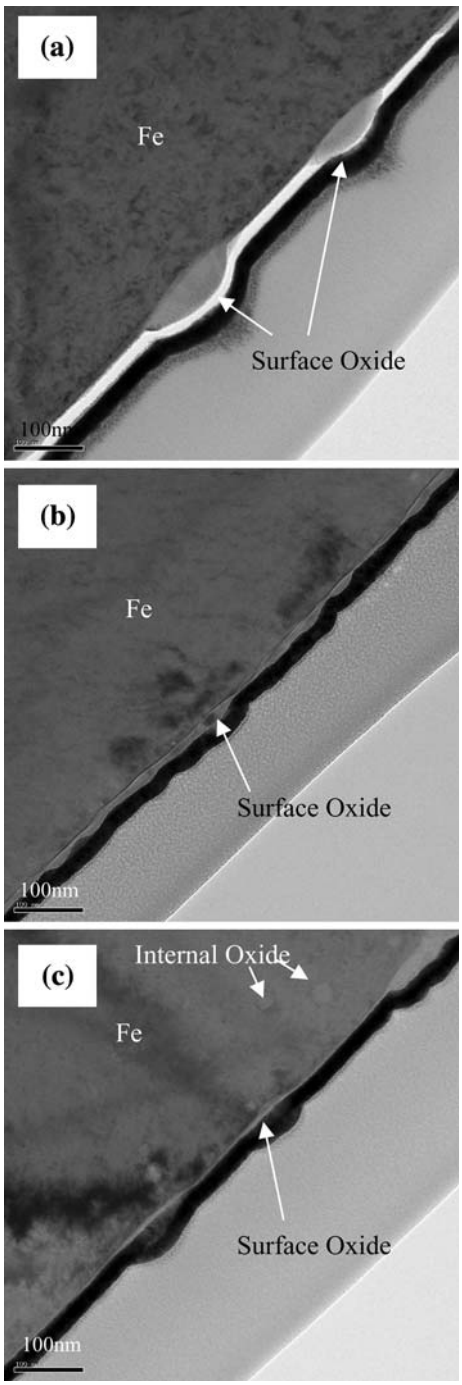

Fig. 3 Cross section of the steel plates annealed at **a** DP −60 °C, **b** DP −40 °C, and **c** DP 0 °C investigated with TEM (bright-field image)

In Figs. 3 and 4, the TEM images of the cross section of the samples are shown. It was found that the surface of the sample annealed at a DP of −60 °C contained isolated large oxide particles on a very thin oxide layer (∼2 nm), whereas that of the sample annealed at a DP of −40 °C contained irregular oxide particles on a relatively thick oxide layer (∼15 nm). The thick oxide layer on the steel

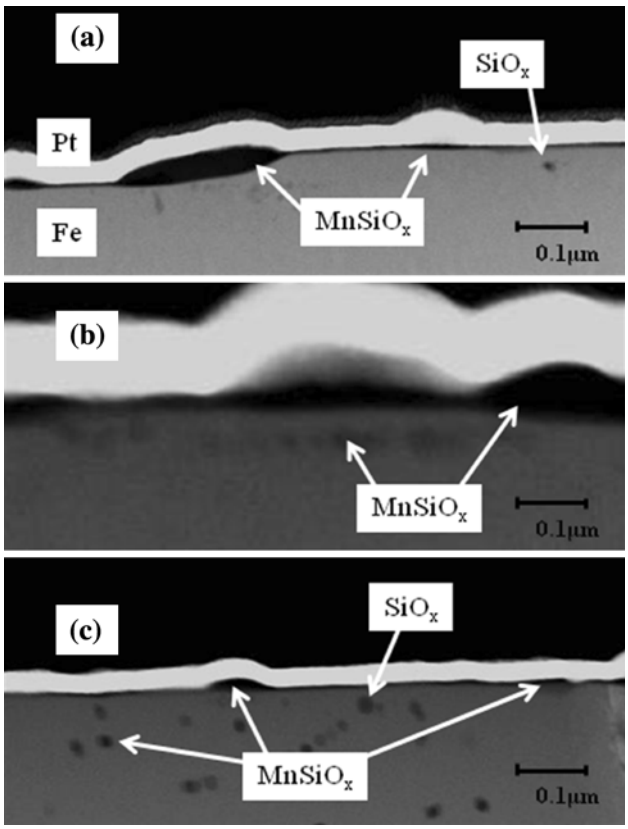

Fig. 4 Cross section of the steel plates annealed at **a** DP −60 °C, **b** DP −40 °C, and **c** DP 0 °C investigated with TEM (HAADF image)

sample annealed at a DP of −40 °C could be explained by the increase in the driving force to form the oxide layer. The mostly noteworthy result was found in the sample annealed at a DP of 0 °C. Although there was a driving force to form the oxide layer on the steel surface, only very small oxide particles were found on a thin oxide layer (1–2 nm). In contrast, many small oxide particles were found in the internal steel matrix indicating that internal oxidation occurred. EDS analysis showed that these particles contain Si or Mn and Si. The oxides formed could be SiO_2 or Mn_xSiO_y (Fig. 5).

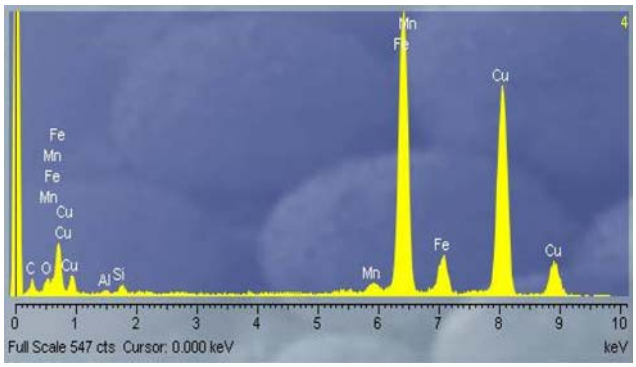

Fig. 5 Typical EDS analysis result of the internal oxides in Fig. 4c

The thin oxide layer can explain the poor wettability in the initial period of wetting, because the initial wetting contact angle is determined from the surface chemistry. For the sample annealed at a DP of 0 °C, diffusion of Fe and Zn through the thin oxide layer was very fast. Therefore, the contact angle could rapidly decrease over time due to the formation of intermetallic compounds [18, 19]. However, for the sample annealed at a DP of −40 °C, diffusion of Fe and Zn through the thick oxide layer was very slow, and the contact angle started to decrease from 10 s. For the sample annealed at a DP of −60 °C, diffusion of Fe and Zn through the thin oxide layer would be of the same order as that at 0 °C. However, big isolated particles occupied some portion of the reaction area, yielding decrease in the reduction rate of the contact angle.

Thermodynamic calculation of the internal oxidation criteria

Mataigne et al. [5] suggested a theoretical model to determine the transition limit between internal and external oxidation based on the Wagner's model [20].

$$\sum N_X^i [nD_X V_{XO_n}]^{1/2} = [0.3\pi V N_O^s D_O/2]^{1/2} \quad (1)$$

where N_X^i is the mole fraction of the alloying element X, n is the ratio between oxygen and metallic atoms in the oxide (1 for MnO and 2 for SiO_2), D_X is the diffusion coefficient of the element X in the alloy, V_{XO_n} is the molar volume of XO_n (13.21×10^{-6} m^3/mol for MnO, 23.72×10^{-6} m^3/mol for SiO_2, and 12.86×10^{-6} m^3/mol for Al_2O_3 [21]), V is the molar volume of iron (7.1×10^{-6} m^3/mol [21]), N_O^s is the surface-adsorbed oxygen molar fraction, and D_O is the diffusion coefficient of oxygen in iron.

The diffusion coefficient of oxygen and alloying elements (Si, Mn, Al) can be described by Arrhenius-type equations [5].

$$D_{Si}(10^{-4}m^2/s) = 8.0 \times \exp\left(-\frac{29{,}945}{T}\right) \quad (2)$$

$$D_{Mn}(10^{-4}m^2/s) = 1.49 \times \exp\left(-\frac{28{,}083}{T}\right) \quad (3)$$

$$D_{Al}(10^{-4}m^2/s) = 5.90 \times \exp\left(-\frac{29{,}171}{T}\right) \quad (4)$$

$$D_O(10^{-4}m^2/s) = 0.0371 \times \exp\left(-\frac{11{,}600}{T}\right) \quad (5)$$

The surface-adsorbed oxygen molar fraction can be calculated from Eq. 6 [5].

$$N_O^s = 0.215 \times \left(\frac{p_{H_2O}}{p_{H_2}}\right) \exp\left(-\frac{11{,}513}{T}\right) \quad (6)$$

Using Eqs. 1–6, for the given alloy (0.3 wt%Si–0.4 wt%Mn) annealed at 800 °C, the critical dew point ($DP_{crit.}$) was determined to be −39 °C. Accordingly, above $DP_{crit.}$, one may expect the surface oxidation would decrease due to the increase in the internal oxidation. The present experimental results shown in Fig. 4 are in reasonable accord with the predicted behavior according to Mataigne's model. Consequently, it is considered that the internal oxidation was pronounced above $DP_{crit.}$ so that only a very thin surface oxide layer of 1–2 nm was formed for the sample annealed at the dew point of 0 °C, and the improvement of the wettability of the steel plate by liquid zinc was caused by the short diffusion distance of the surface oxide layer.

Conclusion

In this study, we investigated the wetting characteristics of the 0.3 wt%Si–0.4 wt%Mn IF-HSS plate by liquid zinc under a 15%H_2–N_2 atmosphere at three different dew points (−60, −40, and 0 °C). It was found that the initial contact angle ($t = 0$ s) was as high as 100–120°, which was explained by the shallow surface oxide layer confirmed by TEM. As the wetting time was increased, the contact angle gradually decreased by the chemical reaction. The surface oxides affect the change in the contact angle, and the wettability of the steel plate annealed at the dew point of 0 °C showed the best performance among the tested samples. The wetting characteristics were coupled with the surface oxides morphology analysis and thermodynamic calculation, and the improvement of the wettability of the steel plate annealed at the dew point of 0 °C was successfully explained by the internal oxidation model.

Acknowledgements We gratefully acknowledge the support of POSCO. Also, J. Park and Y. Kim were supported by the second stage of the Brain Korea 21 Project in 2008 and 2009, respectively.

References

1. Kyono K, Kato C, Sakata K (2003) Kawasaki Steel Tech Rep 35:33
2. Pichler A, Traint S, Arnolder G, Stiaszny P, Blaimschein M, Werner EA (2003) Iron Steelmaker 30(6):21
3. Lee J, Matsuoka K, Shimada S, Tanaka T (2004) 6th international conference on zinc and zinc alloy coated sheet steels. Association for Iron & Steel Technology, Warrendale, p 987
4. Lee J, Park J, Jeon SH (2009) Metall Mater Trans B 40B:1035
5. Mataigne JM, Lamberigts M, Leroy V (1992) In: Pradhan R, Gupta I (eds) Developments in the annealing of sheet steels. TMS, Warrendale
6. Yamashita T, Yamamoto A, Kato C (1994) CAMP-ISIJ 7:388
7. Kato C, Sekine T, Umino S, Yamashita T, Mochizuki K, Masuda M (1994) CAMP-ISIJ 7:1511
8. Cassie ABD (1948) Discuss Frad Soc 3:11
9. Hirose Y, Togawa H, Sumiya J (1982) Tetsu-to-Hagané 68:658
10. Bordignon L (2007) Rev Metall 104:300

11. Zakharova TV, Popel SI (1972) Iz VUZ Chern Metall 3:17
12. Ebrill N, Durandet Y, Strezov L (2000) Metall Mat Trans B 31:1069
13. Shimada S, Takada Y, Lee J, Tanaka T (2008) ISIJ Int 48:1246
14. Takada Y, Shimada S, Lee J, Kurosaki M, Tanaka T (2009) ISIJ Int 49:100
15. Li XS, Baek S-I, Oh C-S, Kim S-J, Kim Y-W (2008) Scripta Mater 59:290
16. Khondker R, Mertens A, McDermid JR (2007) Mater Sci Eng A 463:157
17. Gong YF, Kim HS, De Cooman BC (2008) ISIJ Int 48:1745
18. Protsenko P, Terlain A, Traskine V, Eustathopoulos N (2001) Scripta Mater 45:1439
19. Ueda S, Taguchi O, Iijima Y, Takahashi G, Yamaguchi K (2008) J Mater Sci 43:5666. doi:10.1007/s10853-008-2767-y
20. Wagner C (1959) Z Elektrochem 63:772
21. Lide DR (2005–2006) CRC handbook of chemistry and physics. Taylor & Francis, Boca Raton